MethodsX 12 (2024) 102744

Contents lists available at ScienceDirect

MethodsX

journal homepage: www.elsevier.com/locate/methodsx

Investigation of red clay and waste glass composite bricks for ionizing radiation shielding

Delphine K. Nzivulu*, Nadir O. Hashim, Nicholas Musila, Kapis E. Otieno, Felix O. Wanjala

Physics Department, Kenyatta University, P.O BOX 43844, Nairobi, Kenya

A R T I C L E I N F O

Method name:
Gamma-ray spectroscopy

Keywords:
Ionizing radiation
Red clay, and glass (RCG)
Control sample (CNT)
Gamma-ray spectroscopy
Linear attenuation coefficient (μ)
Mass attenuation coefficient
Half value layer (HVL)
Mean free path (MFP)

A B S T R A C T

Ionizing radiation is valuable for healthcare, industry, and agriculture. However, excessive exposure to ionizing radiation is detrimental to humans and the environment. Radiation protection aims at protecting people and the environment from the harmful effects of ionizing radiation. This work aimed to study the effectiveness of composites of red clay and waste glass for ionizing radiation shielding. Five samples of different mix ratios of red clay to waste glass were fabricated into different dimensions using hand molding, dried, and burnt. The samples were characterized for ionizing radiation shielding. Monte-Carlo simulation was done using the GEANT4 toolkit and web-based NIST-XCOM photon attenuation database. The findings show that the measured half value layer (HVL) for the composite bricks showed a linear decrease from (6.13± 0.10) cm for the CNT sample that had 0 % waste glass to (4.62± 0.12) cm for the RCG11 sample that had 50 % waste glass. The GEANT4 simulated HVL values for CNT and RCG11 samples were (6.05±0.01) cm and (4.79±0.01) cm respectively. The NIST-XCOM values were (6.09±0.09) cm and (4.81± 0.01) cm for CNT and RCG11 respectively. The measured and simulated results were in good agreement. The findings of this study indicate an improvement in the shielding properties of red clay with the addition of waste glass and will promote radiation safety by providing an environmentally friendly alternative shielding material.

- Proper shielding is key in promoting radiation safety and protection. There is a need for alternative shielding materials that can be used for walling during the construction of structures that house radioactive materials.
- Red clay and waste glass composite bricks can provide alternative ionizing radiation shielding material.
- This study will promote environmentally friendly practices in radiation safety and protection.

Specifications table

Subject area:	Physics and Astronomy
More specific subject area:	Ionizing radiation shielding
Name of your method:	Gamma-ray spectroscopy
Name and reference of the original method:	Characterization of red clay and glass composite for ionizing radiation shielding
Resource availability:	Data is available in this article

* Corresponding author.
E-mail address: nzivulukasyoka@students.ku.ac.ke (D.K. Nzivulu).
Social media: (D.K. Nzivulu)

https://doi.org/10.1016/j.mex.2024.102744
Received 8 February 2024; Accepted 2 May 2024
Available online 3 May 2024

Method details

Introduction

Gamma rays are being used more frequently in sectors like nuclear medicine, medical physics, bioscience, as well as material research [1–4]. Gamma radiation exposure over an extended period can harm living cells and tissues [1]. Ionizing radiation-related adverse health consequences can be divided into deterministic effects as well as stochastic effects. The As Low As, Reasonably Achievable (ALARA) principle, was developed in 1977 by the International Commission on Radiation Protection (ICRP). It provides guidelines for minimizing exposure to ionizing radiation. This is achieved by limiting the exposure time, increasing the distance from the radiation source, and using the right shielding material for ionizing radiation shielding.

Materials that are effective as a shield against ionizing radiation will absorb, scatter, or block the majority of the incident radiation. The use of suitable shielding is one of the principles of radiation protection [1]. The type and intensity of incident radiation determine the choice of material that would be suitable for radiation shielding. The selection of shielding materials should be based on their radiation damage resistance, physical toughness, ease of manufacture, and relative affordability [5]. The coefficient of linear attenuation is a measure of the fraction of a gamma ray beam that is absorbed or dispersed per unit thickness of the absorber material. It is used to evaluate or assess the effectiveness of the material for shielding. Materials like lead, steel, and concrete are the most commonly used shields against ionizing radiation [5]. Ongoing research explores nanomaterials and advanced composites for enhanced shielding properties [6]. These materials aim to provide improved protection while addressing the limitations associated with traditional shielding materials.

Red clay bricks have gained attention for their potential in radiation shielding. This study explores how these bricks, commonly used in construction, exhibit properties that make them effective at attenuating ionizing radiation. Red clay bricks are primarily composed of clay minerals, silica, alumina, and iron oxide. Studies have specifically evaluated the gamma-ray shielding behavior of burnt red clay bricks across a broad energy range. The results demonstrate their efficacy in attenuating gamma rays, making them suitable for applications in storage facilities and other settings where radiation protection is essential [7]. Ongoing research into enhancements, such as nanoparticle grafting, further expands the potential applications of red clay in the field of radiation shielding. This study has used narrow beam geometry to examine the linear attenuation coefficient of red-clay and glass composite brick at 662 keV gamma-ray energy. This was used to evaluate the HVL and Mean-Free-Path (MFP) for photons of this energy. These parameters are considered in evaluating the effectiveness of a shield in radiation protection.

Materials and methods

Red clay was collected from the Siembeni area in the Kibwezi sub-county, Makueni County, Kenya. The waste glass was from waste household glass bottles. Spectroscopic photon attenuation measurements were carried out at the Kenya Bureau of Standards, using a model SC10–1–12 Gamma Beam Irradiator supplied by Hopewell Designs.INC. The irradiator was available with a well-collimated Cs-137 source and additional collimators for different beam sizes. A digital sodium iodide scintillation detector was used for quantitative assessment of the transmitted intensity.

Sample collection and preparation

Red clay was crushed into appropriate sizes and sieved through a 2 mm screen. Waste glass bottles were crushed into powder and sieved through a 2 mm sieve mesh. Clay powder and glass granules were combined. Different mix ratios of red-clay to glass were used, the mix ratios were 0 %,20 %, 25 %, 33.33 %, and 50 % waste glass for CNT, RCG41, RCG31, RCG21, and RCG11 samples respectively. The bricks were made through hand molding. A rectangular brick form was used to provide a range of RCG sample thicknesses. The samples were dried and burned in an electric laboratory furnace at 1000 ˚C with a ramping rate of 3 ˚C/min and a holding time of 30 min.

Sample analysis

Linear attenuation coefficient

The reduction in radiation intensity that occurs as radiation passes through a target material is quantified by the linear attenuation coefficient (μ). It is based on the density of the absorber material. From the Beer-Lambert law given in Eq. (1), Eq. (2) is derived. The linear attenuation coefficient was determined graphically for Eq. (2).

$$N = N_0 e^{-\mu x} \tag{1}$$

$$lnN = -\mu x + lnN_O \tag{2}$$

where x is the thickness of the absorber material, N_o is the intensity of incident photon energy before attenuation and N is the transmitted intensity.

Narrow beam gamma-ray spectroscopy was used. The experimental setup is shown in Fig. 1. Laser beams were used for the alignment to ensure the correct positioning of the source, sample, and detector. A video camera for instrument and room viewing

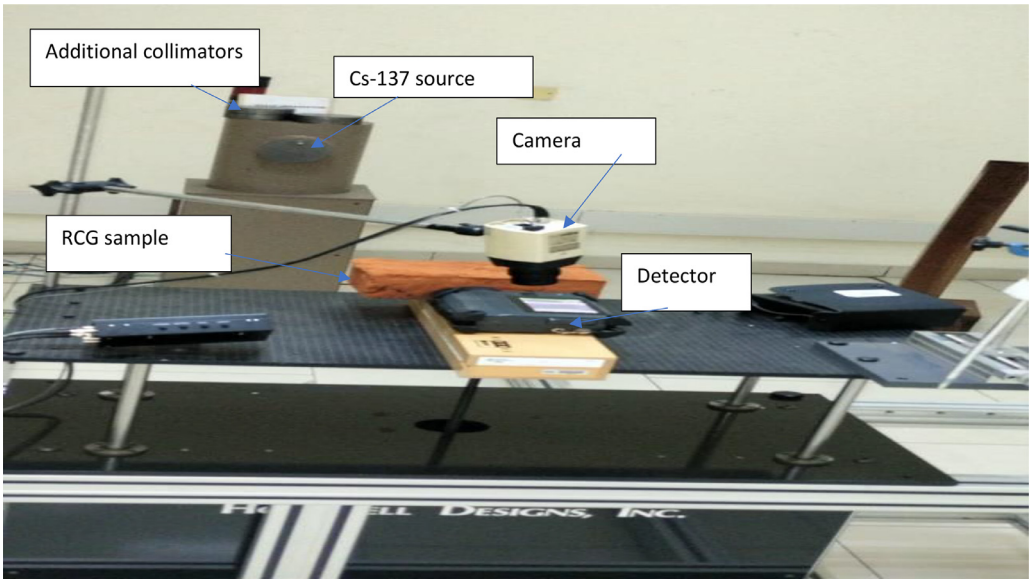

Fig. 1. Experimental setup at Kenya Bureau of Standards.

was used. The position stand held the sample and detector in position. RCG samples were placed at a distance of 200 cm from the Cs-137 source. After exposure, live counts were recorded from the computer display. Approximately after 120 s of exposure, the net counts per second at the photo peak energy of 662 keV were recorded.

The linear attenuation coefficient affects the half-value layer (HVL). The transmitted photon intensity drops to half its initial intensity at this minimum thickness of the material. The half value layer (HVL) which is the thickness of the sample that will reduce the gamma radiation to half the initial intensity was calculated from Eq. (2).

$$HVL = \frac{ln\,2}{\mu} \tag{3}$$

The mean free path (MFP) is the relaxation length. It gives the average distance a single particle travels through a given attenuating medium before interacting with it. It depends on the material properties and the energy of the photon. It is related to the linear attenuation coefficient by Eq. 4.

$$\psi_m = \frac{1}{\mu} \tag{4}$$

Mass attenuation coefficient

The mass attenuation coefficient is a measure of the ability of a material to absorb or scatter incident electromagnetic radiation per unit mass and is independent of the density as given in Eq. 5. It provides important information in determining how best the material can attenuate a given photon energy and the possibilities of application in radiation shields [8]. The mass attenuation coefficient is a crucial factor to consider when researching how radiation interacts with matter because the linear attenuation coefficient is dependent on the density of the substance being used. The mass attenuation coefficient indicates how much energy is dispersed or absorbed within a target material of a specific effective thickness. The size of the linear attenuation coefficient relies on the incident photon energy, the chemical composition, the bonding, and characteristics like the thickness and density of the absorber material. The sum of the weight fraction as well as the mass attenuation coefficient of the i^{th} element, yields the mass attenuation coefficient of the composite at specific energy. This is described in Eq. (5).

$$\left(\frac{\mu}{\rho}\right) = \sum w_i \left(\frac{\mu}{\rho}\right)_i \tag{5}$$

where w_i and $(\frac{\mu}{\rho})_i$ are the fractional weight and total mass attenuation coefficient of the i^{th} constituent element. Energy Dispersive X-ray spectroscopy (EDX) was used to calculate the elemental concentration of the composites.

EDX-spectroscopy

The elemental concentrations of the sample were analyzed using an Energy Dispersive X-ray spectroscopy machine (EDX 800-HS). The samples were pulverized for analysis in air mode and put in a sample cell. The detector was cooled by liquid Nitrogen in Nitrogen. Energy calibration for the detector was carried out using internal standard A750 which is an accessory of the machine. Analyses of the measured spectra were carried out to estimate the chemical composition of the samples.

GEANT4 simulation

Monte Carlo simulation was done using the Geometry and Tracking Version 4 (GEANT4) toolkit. The geometry was defined and G4 material was defined using the elemental concentration of the samples as obtained from EDX-spectroscopy. The nature of the particle was defined as gamma and beam energy set at 662 keV. Each sample was irradiated with 100,000 photons at the set energy. During each run one file was called at a time using the macro files in the batch process.

NIST-XCOM simulation

The NIST- XCOM Database is a web-based resource that allows users to calculate photon cross-sections for different processes such as scattering, photoelectric absorption, and pair production [9]. The percentage elemental concentrations of each sample were used as input for the web-based photon attenuation database NIST-XCOM. The energy range is set at default whose range is 1 keV to 100 GeV. The mixture rule is applied in the XCOM program to find the total and partial mass attenuation coefficients for both compounds, elements, and mixtures for photon energies [3]. On submitting, the system automatically calculated the mass attenuation coefficient. The database provides output information of attenuation graphs which can be downloaded and text files which can be analyzed.

Compressive strength test

To establish whether the bricks were suitable building materials, the compressive strength was examined through a destructive method. This was accomplished by inserting a brick between the testing machine's plates with its flat faces horizontal and its mortar-filled face facing upward. Up until failure, a load was applied axially at a constant rate, and the greatest load at failure was recorded. Compressive strength was determined from Eq. (6). The results were compared to the Kenyan set standard (Kenya standard DKS 2801–1:2019) brick specification for masonry units (clay masonry units).

$$Compressive\ strength\ of\ a\ brick = \frac{Maximun\ load\ at\ failure(N)}{Average\ area\ of\ bed\ face\ \left(mm^2\right)} \tag{6}$$

Water absorption test

The tendency of a brick to absorb water is one measure of a brick's durability. The less the amount of water a brick absorbs the greater the resistance to weathering, this increases its durability [10]. The absorption test was used to determine how much moisture content can be absorbed under difficult circumstances. A dry brick's weight was recorded as (m_1), and the brick was then submerged in water for 24 h. Weighing the brick once more was done and recorded as (m_2). Water was absorbed due to the dry and wet bricks' different weights. The value obtained was contrasted with the Kenyan standard design (Kenya standard DKS 2801–1:2019). Eq. (7) was used to evaluate the water absorption of each sample.

$$W_a = \frac{m_2 - m_1}{m_1} \times 100 \tag{7}$$

Method validation

Results and discussion

Linear attenuation measurements

The count rate was obtained at 662 keV peak energy. The data recorded gave the highest count rate of 883.17 cps without the attenuator. Which is the incident photon intensity (N_o). A linear decrease in the count rate was noted as the absorber thickness increased. This could be a result of photon interactions with a large number of sub-atomic particles mainly through the Compton effect which is predominant at intermediate energies [1].

The natural logarithm of the transmitted intensity against the sample thickness for the five samples was plotted on the same canvas using Jupiter notebook as shown in Fig. 2. From Eq. 2 the slope of each of the five graphs gave the linear attenuation coefficient. A comparison of the samples indicates that RCG11 whose slope was steepest had the highest linear attenuation coefficient as obtained from the measured data. The measured linear absorption coefficient ranged from 0.113 ± 0.011 cm^{-1} for the CNT sample that had 0 % glass to 0.150 ± 0.018 cm^{-1} for the RCG11 sample that had 50 % glass.

Table 1 provides the linear attenuation coefficient for all samples from measured data. There was a significant increase in linear attenuation values with the addition of waste glass. Since the linear attenuation coefficient is a parameter that characterizes the radiation shielding property of a material, this suggests that waste glass addition to red clay bricks improves the shielding properties of the composite brick. RCG11 sample is the best gamma ray shielding material of the five samples under this study based on measured data. Waste glass increased the physical density of the samples. There was a linear relationship between the physical density and the linear attenuation coefficient for materials [2].

GEANT4 simulated linear attenuation coefficient

The results obtained from the simulation were in good agreement with measured values. The range of absorption coefficient values was (0.115 ± 0.001) (cm^{-1}) for the CNT sample to (0.145 ± 0.001) (cm^{-1}) for the RCG11 sample. Table 1 provides values for all samples. A comparative graph was plotted to compare the measured and simulated values as shown in Fig. 3.

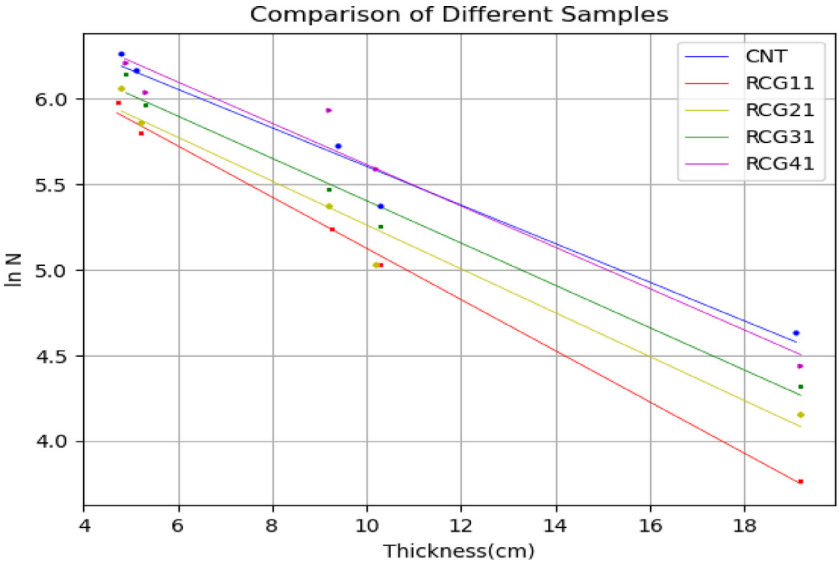

Fig. 2. Linear fit of natural logarithm of transmitted intensity against sample thickness.

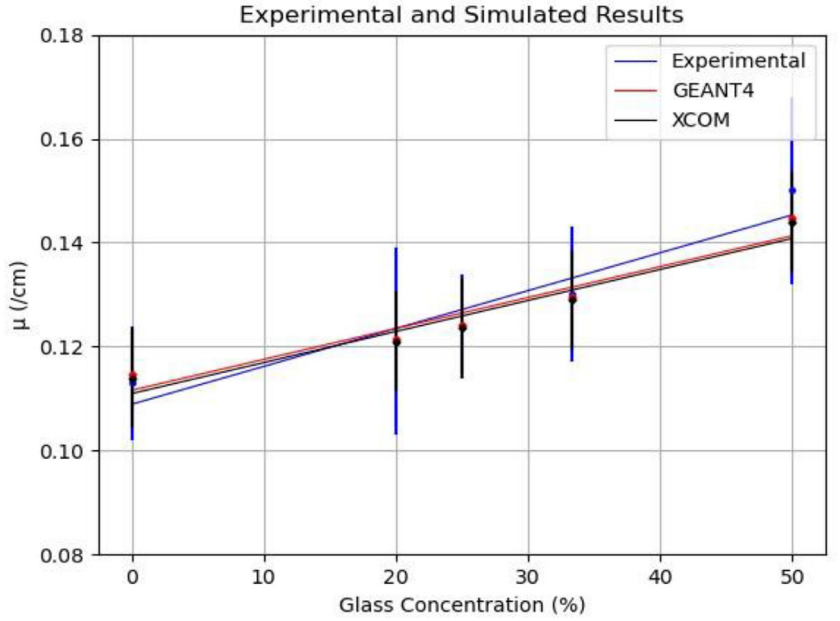

Fig. 3. Comparison of simulated and measured linear attenuation coefficient.

Table 1
Measured, GEANT4 and NIST-XCOM linear attenuation coefficient.

Sample	Measured μ (cm^{-1})	GEANT4 μ (cm^{-1}) ±0.001	NIST-XCOM μ (cm^{-1}) ±0.009
CNT	0.113 ± 0.011	0.115	0.114
RCG11	0.150 ± 0.018	0.145	0.144
RCG21	0.130 ± 0.013	0.130	0.129
RCG31	0.125 ± 0.010	0.124	0.124
RCG41	0.121 ± 0.018	0.121	0.121

Table 2
Measured, GEANT4 and NIST-XCOM HVL and MFP.

Sample	Measured		GEANT4		NIST-XCOM	
	HVL (cm)	MFP (cm)	HVL (cm) ±0.01	MFP (cm) ±0.001	HVL (cm) ±0.01	MFP (cm) ±0.004
CNT	6.13 ± 0.10	8.85 ± 0.01	6.05	8.724	6.09	8.780
RCG11	4.62 ± 0.12	6.67 ± 0.02	4.79	6.916	4.81	6.944
RCG21	5.33 ± 0.10	7.69 ± 0.01	5.35	7.721	5.37	7.752
RCG31	5.55 ± 0.08	8.06 ± 0.01	5.59	8.061	5.61	8.097
RCG41	5.73 ± 0.15	8.26 ± 0.02	5.71	8.233	5.74	8.264

Table 3
comparison of mass attenuation coefficient and HVL values from this work and published data measured at 662 keV.

Material	Density (g/cm^3)	Mass attenuation coefficient (cm^2/g)	HVL (cm)
CNT	1.52	0.074 ± 0.011	6.13 ± 0.10
RCG41	1.61	0.075 ± 0.018	5.73 ± 0.15
RCG31	1.64	0.076 ± 0.013	5.55 ± 0.08
RCG21	1.71	0.076 ± 0.010	5.73 ± 0.15
RCG11	1.90	0.079 ± 0.018	4.62 ± 0.12
Concrete (Dogan and Altinsoy, 2015)	2.25	0.081	3.8
Ordinary concrete (Sharifi et al. 2013)	2.30	0.079	3.8
Brick (Dogan and Altinsoy, 2015)	1.50	0.076	6.1
Barite (Sharifi et al. 2013)	3.35	0.078	2.6
Serpentine (Sharifi et al.2013)	2.60	0.082	3.2

XCOM simulated linear attenuation coefficient

The system automatically calculated the mass attenuation coefficient of the samples and provided analysis graphs for the photon interactions. The linear attenuation coefficients were evaluated using Eqn 5. Table 1 gives the linear attenuation coefficient of the five RCG samples as determined from this simulation. The linear attenuation coefficient increased from (0.114±0.009) (cm^{-1}) for CNT to (0.144±0.009) (cm^{-1}) for the RCG11 sample. The results from this simulation are also in good agreement with those obtained experimentally.

The three graphs indicate a linear increase in the linear attenuation coefficient as the percentage of glass increased. The linear attenuation of the RCG11 sample was highest across the three methods used. Since the linear attenuation coefficient is a measure of the fraction of incident gamma ray beam that one centimeter of a material attenuates, then this implies that of the five samples studied this was the best shielding material.

The measured and simulated linear absorption values were used to determine the HVL and MFP according to Eqs. (3) and (4). The HVL values from the GEANT4 simulation were (4.79±0.01) cm for the RCG11 sample and (6.05 ± 0.01) cm for the CNT sample, the corresponding MFP values were (6.916 ± 0.001) cm and (8.724 ± 0.001) cm respectively. From the NIST-XCOM simulation, the HVL values for RCG11 and CNT samples were (4.81 ± 0.01) cm and (6.09 ± 0.01) cm respectively. The corresponding MFP values were (6.944 ± 0.004) cm and (8.780 ± 0.004) cm respectively. Table 2 provides the HVL and MFP values for the other samples under this study.

The mass attenuation measurements were determined using Eq. (5). RCG11 had the highest mass attenuation coefficient (0.079 ± 0.018) (cm^2/g), while CNT had the lowest mass attenuation coefficient of (0.074 ± 0.011) (cm^2/g). The increased attenuation coefficient was a result of increased physical density as a consequence of increased% waste glass, this increased the number of atoms for interaction thereby raising the probability of photon-matter interaction. RCG11 sample whose density was (1.901 ± 0.002) g/cm^3 had a higher mass attenuation coefficient compared to ordinary concrete of density 2.38 g/cm^3 that had a mass attenuation coefficient of 0.07017 (cm^2/g) measured at 662 keV [11].

Table 3 compares the HVL and experimental mass attenuation data from this research with other published data. The experimental mass attenuation coefficient and HVL values for the brick sample agree with the CNT results from this work [12]. The mass attenuation coefficient of ordinary concrete compares well with that of the RCG11 sample that had 50 % glass [13].

Compressive strength test

According to the Technical Committee on Kenya Standards (DKS 2801–1:2019) the required compressive strength for load-bearing category masonry units is 7 N/mm^2. All the RCG samples met this requirement as shown in Table 4. The compressive strength was extremely dependent on the amount of waste glass in the composites, this result agrees with published results [10,14,15]. This could be attributed to the non-crystalline nature of glass which encourages sintering during heating hence a stronger brick. Moreover, as the percentage of waste glass increased in subsequent samples the bulk density increased as the water absorption decreased this contributed to increased compressive strength [10]. Waste glass addition brought in a glass phase transformation in the body that contributed to vitrification and enhanced strength development by closing internal pores. During heating this liquid glassy phase acts as a binder which promotes a more compact microstructure with fewer pores, voids, and fractures delivering better physical and

Table 4
Compressive strength test and water absorption test values.

Sample	Compressive strength (N/mm^2)	Water absorption%
CNT	7.12 ± 0.07	18.87 ± 0.03
RCG41	7.89 ± 0.07	17.59 ± 0.04
RCG31	8.51 ± 0.09	16.86 ± 0.03
RCG21	9.26 ± 0.09	15.75 ± 0.03
RCG11	10.30 ± 0.01	12.91 ± 0.02

mechanical properties to the material [15]. The compressive strength was least in the CNT sample that had 0 % waste glass, this is attributed to increased porosity compared to the other samples that had waste glass (Table 4).

Water absorption

In this study, the dry weight of each sample was recorded. The composite bricks were immersed in water for 24 h and weighed again. The water absorption test was determined using Eqn 7. Since glass absorbs less water than clay, as the percentage of waste glass increased in the samples the water absorption significantly decreased. Table 4 provides% water absorption for the various samples. All RCG samples met the Kenyan standard for masonry units of 12 % −20 % (DKS 2801–1:2019). Other published work on red clay bricks with waste glass addition shows a decrease in water absorption as waste glass increased [10,16]. Water absorption is directly related to apparent porosity; therefore, the internal structure of bricks should be dense enough to avoid water intrusion [14]. The addition of waste glass contributed to the densification of the clay brick, thereby reducing the water absorption resulting in increased durability of the samples [17]. Increasing the waste glass content enhances the formation of liquid-phase glass resulting in reduced voids and pore volume in the material [15,17]. This caused the water absorption rate CNT sample to be higher compared to the other samples that had waste glass. Also, the decrease in water absorption with a% increase in waste glass is attributed to increased compactness of particles due to vitrification of bricks and partial glassification of clay during burning leading to reduced absorption in subsequent samples with higher% of waste glass [18].

Conclusion

The objective of this study was to fabricate and characterize red clay and waste glass composite bricks with different mix ratios for ionizing radiation shielding. The analysis from measured data indicates a linear decrease in transmitted intensity as the percentage of glass increases in subsequent composites up to 50 % waste glass. The HVL and MFP values of the five samples under study make them suitable for ionizing radiation shielding. The simulated data agreed well with the measured data. This shows that RCG samples can provide alternative ionizing radiation shielding material for use in walling during the construction of buildings that house radioactive sources since they passed the basic requirements for masonry bricks. The use of these composite bricks would promote environmentally friendly practices in radiation protection and safety through the recycling of waste glass bottles.

Ethics statement

This work did not involve animal experiments or the collection of data from social media platforms.

Declaration of competing interest

The authors declare that they have no known competing financial interests or personal relationships that could have appeared to influence the work reported in this paper.

CRediT authorship contribution statement

Delphine K. Nzivulu: Conceptualization, Formal analysis, Data curation, Methodology, Writing – original draft. **Nadir O. Hashim:** Conceptualization, Supervision, Funding acquisition, Formal analysis, Writing – review & editing. **Nicholas Musila:** Conceptualization, Supervision, Funding acquisition, Formal analysis, Writing – review & editing. **Kapis E. Otieno:** Writing – review & editing. **Felix O. Wanjala:** Conceptualization, Supervision, Funding acquisition, Formal analysis, Writing – review & editing.

Data availability

Data will be made available on request.

Acknowledgments

This work was carried out in the Department of Metrology at the Kenya Bureau of Standards. Radiation detectors used in this work were provided by the International Atomic Energy Agency (IAEA) through the Division of Technical Cooperation under the project RAF 2012.

References

[1] E.B. Podgorsak, Radiation Oncology Physics, IAEA, Vienna, 2005.
[2] E. Halliwell, C. Couch, R. Begum, W. Li, M. Maqbool, Increase in linear attenuation coefficient by changing crystal structure of materials for radiation shielding and biomedical devices safety, Colloids Surf. A Physicochem. Eng. Asp. 622 (2021) 126646.
[3] Pondo, J. (2019). Monte-Carlo simulation and measurement of gamma ray attenuation in concrete. Master of Science Thesis. Kenyatta University, Kenya.
[4] A.M. Babeer, H.Y. Amin, M.I. Sayyed, A.E.R. Mahmoud, M.S. Sadeq, Impact of glass matrix Sb2O3–NiO–Na2O–B2O3 on the structure, optical, ligand field characteristics and radiation shielding parameters of borate glass system, Ceram. Int. 50 (2024) 17439–17451.
[5] S. Yasmin, B.S. Barua, M.U. Khandaker, M.A. Rashid, D.A. Bradley, M.A. Olatunji, M. Kamal, Studies of ionizing radiation shielding effectiveness of silica-based commercial glasses used in Bangladeshi dwellings, Results Phys. 9 (2018) 541–549.
[6] M. Elsafi, M.F. Dib, H.E. Mustafa, M.I. Sayyed, M.U. Khandaker, A. Alsubaie, A.M. El-Khatib, Enhancement of ceramics based red-clay by bulk and nano metal oxides for photon shielding features, Materials, 14 (24) (2021) 7878.
[7] K.S. Mann, M.S. Heer, A. Rani, Investigation of clay bricks for storage facilities of radioactive-wastage, Appl. Clay Sci. 119 (2016) 249–256.
[8] Otieno, K. (2019). Gamma and X-ray shielding potential of Styrene Butadiene rubber polymer filled with lead (ii) oxide composites for radiation protection. Master of Science Thesis. Kenyatta University, Kenya.
[9] Berger, M.J.K (2010). XCOM: Photon cross sections database. http://www.nist.gov/pml/data/xcom/index.cfm.
[10] M.R. Hasan, A. Siddika, M.P.A. Akanda, M.R. Islam, Effects of waste glass addition on the physical and mechanical properties of brick, Innov. Infrastruct. Solut. 6 (2021) 1–13.
[11] V. Fugaru, S. Bercea, C. Postolache, S. Manea, A. Moanta, I. Petre, M. Gheorghe, Gamma ray shielding properties of some concrete materials, Acta Phys. Pol. A 127 (4) (2015) 1427–1429.
[12] B. Dogan, N. Altinsoy, Investigation of photon attenuation coefficient of some building materials, AIP Conf. Proc. 1653 (2015) 020033 (2015.
[13] S. Sharifi, R. Bagheri, S.P. Shirmardi, Comparison of shielding properties for ordinary, barite, serpentine and steel–magnetite concretes using MCNP-4C code and available experimental results, Ann. Nucl. Energy 53 (2013) 529–534.
[14] I. Demir, Reuse of waste glass in building brick production, Waste Manag. Res. 27 (6) (2009) 572–577.
[15] P. Ponce Peña, M.A. González Lozano, A. Rodríguez Pulido, R.H. Lara Castro, Z.V. Quiñones Jurado, J.C. Pérez Medina, A. Villavicencio Torres, Effect of crushed glass cullet sizes on physical and mechanical properties of red clay bricks, Adv. Mater. Sci. Eng. (2016) 4.
[16] S.E. Chidiac, L.M. Federico, Effects of waste glass additions on the properties and durability of fired clay brick, Can. J. Civ. Eng. 34 (11) (2007) 1458–1466.
[17] N. Phonphuak, S. Kanyakam, P. Chindaprasirt, Utilization of waste glass to enhance physical–mechanical properties of fired clay brick, J. Clean. Prod. 112 (2016) 3057–3062.
[18] A. Hameed, S. Abbas, A.U. Qazi, U. Haider, Effect of waste glass on properties of burnt clay bricks, Pak. J. Eng. Appl. Sci. 22 (2018) 56–63.